RESERVE

D5.7 v1.0

Report on the 100% Renewable Grid Scenario, V2

The research leading to these results has received funding from the European Union's Horizon 2020 Research and Innovation Programme, under Grant Agreement no 727481.

Project Name	RESERVE
Contractual Delivery Date:	30.09.2019
Actual Delivery Date:	30.09.2019
Contributors:	Markus Mirz (RWTH), Steffen Vogel (RWTH), Lucian Toma (UPB), Alvaro Ortega Manjavacas (UCD)
Workpackage:	WP5 – Test-beds for validation of research results
Security:	PU
Nature:	R
Version:	1.0
Total number of pages:	37

Abstract:

This report describes the simulations performed to investigate a futuristic scenario towards 100% renewable in a large grid based on real data from the Romanian and the Irish transmission system as well as the Irish distribution system. The conclusions derived from the simulation results are essential feedback for the further development of the control and simulation techniques.

Keyword list:

Laboratory, Infrastructure, pan-European, Co-simulation, Romania, Ireland, 100% Renewable

Executive Summary

The research topics of RESERVE include frequency and voltage control concepts for future grids as well as simulation techniques to enable large-scale distributed real-time co-simulation. The objective of this deliverable is to describe how the control concepts proposed by WP2/3 and the co-simulation platform developed in WP4 are used to support futuristic scenarios of 100% renewables grids.

The presented simulation scenarios are conducted with grid data of the Irish transmission and distribution system and of the Romanian transmission systems. The Irish transmission grid gives insights into the impact of the control techniques on an isolated grid. The Romanian transmission system data is more representative than the Irish transmission system for most European countries which are interconnected with neighboring grids. The two cases complement each other to give a more comprehensive result. Therefore, the deliverable title was changed from “Report on the 100% Renewable Irish Grid Scenario” to “Report on the 100% Renewable Grid Scenario”.

The transmission system results obtained from simulations using the real grid data show how to identify components that can actively participate in the frequency control by applying the frequency maker index described in Deliverables D2.6 and D2.7 and how energy storages in particular can be employed for frequency control. The distribution system simulations focus on voltage control and how converter interfaced components can participate. It is shown that the active voltage management algorithm (AVM) described in D3.1 improves the voltage band in terms of phase imbalances. The virtual output impedance (VOI) introduced in D3.5 control is presented to solve problems related to harmonic instability.

Authors

Partner	Name	e-mail
RWTH		
	Markus Mirz	mmirz@eonerc.rwth-aachen.de
	Steffen Vogel	stvogel@eonerc.rwth-aachen.de
UPB		
	Lucian Toma	lucian.toma@upb.ro
UCD		
	Alvaro Ortega Manjavacas	alvaro.ortegamanjavacas@ucd.ie

Table of Contents

1. Introduction

Renewables in a Stable Electric Grid (RESERVE) is a three-year European Commission funded project within the Work Program H2020-LCE-2016-2017. The project officially started in October 2016.

1.1 Change of Title

The original description of the deliverable stated that the Irish grid would be used for a 100% renewables scenario. It was decided to deviate from this objective and include Romanian transmission system data. In contrast to the Irish transmission system, the Romanian system has strong synchronous interconnections with other continental European countries. Therefore, the inclusion of the Romanian data does have advantages in that it makes the simulation case more representable for the situation of the majority of European countries. However, the isolated grid of Ireland presents also an interesting scenario to test the transition to renewable generation and low-inertia. Therefore, it was decided to present results for both grids in this second version of deliverable D5.6.

1.2 Task 5.4

This deliverable is the second output of Task 5.4 in WP5 updating and replacing Deliverable D5.6 which already described some of the scenarios but did not include any simulation results. Task 5.4 is about simulation based on realistic grid data and focusing on renewables. The concepts developed in WP2/3 are used in these simulations as well as the simulation platform of WP4 to support a high share of renewables. The considered grids are derived from real grid data of the Romanian TSO and Irish TSO/DSO. Therefore, the simulation scenarios are more realistic than previous simulations conducted in the frame of RESERVE which were based on benchmark grids. Compared to offline simulation studies, the real-time simulation presented in this deliverable allow for the integration of communication network equipment and power system field devices in hardware-in-the-loop experiments. In contrast, offline simulations which are not running at wall-clock time speed cannot be applied in hardware-in-the-loop experiments.

1.3 Objectives of the Work Report in this Deliverable

The main objective of this report is the presentation of the simulation results related to 100% renewables and using real grid data. It is explained what grid data and WP2/3 control techniques have been implemented and how the WP4 simulation infrastructure is used to support the evaluation of new techniques.

1.4 Outline of the Deliverable

The first section describes the grid data used in the following simulations. Compared to the previous version, deliverable D5.6, this section has been extended by a subsection about the Irish transmission system data. The description of the Romanian transmission system and Irish distribution system has not changed.

Sections 3 and 4 describe the conducted experiments with details of the simulator setup, the electrical models and the applied control technique.

1.5 How to Read this Document

This document can be read on its own, but should the reader want to learn about the concepts implemented on the co-simulation platform or the architecture of the co-simulation platform itself, it is recommended to read deliverables from WP2/3/4 before. Overall, this deliverable (D5.7) is related to other documents in the RESERVE project as depicted in Figure 1.1.

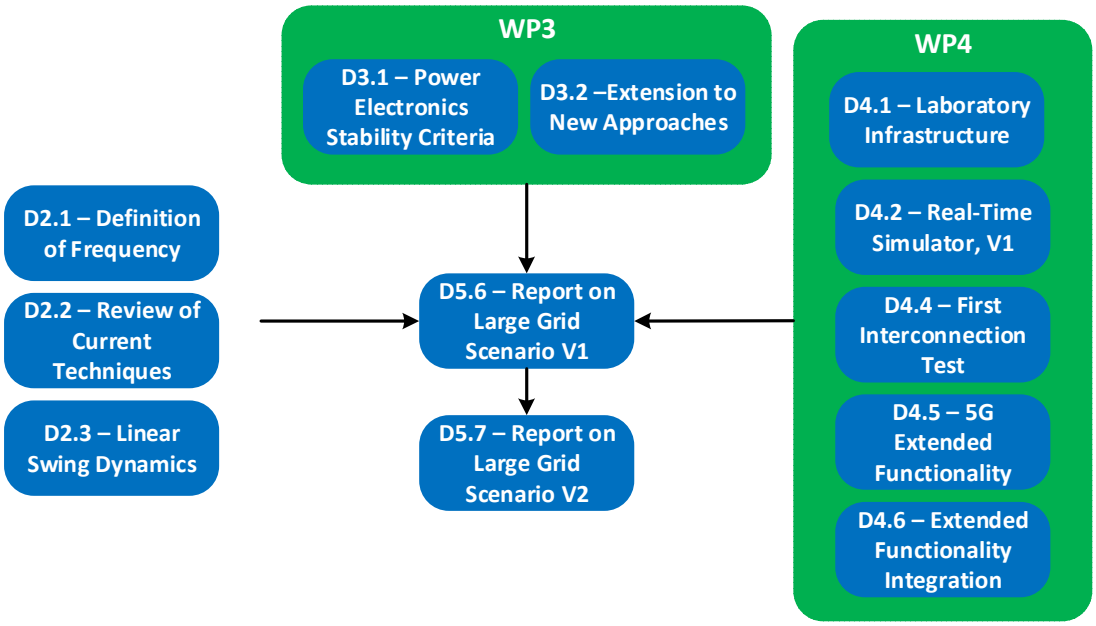

Figure 1.1: Relations between this deliverable and other work

2. The Simulated Power System

The realistic grid scenarios investigated in Task 5.4 include three different grid models:

- A transmission system derived from the Romanian data set of TransE extended with medium voltage (MV) level components for frequency control applications
- A transmission system derived from the Irish data set of EirGrid extended with MV level components for frequency control applications
- A distribution grid based on a low voltage (LV) feeder from the Irish distribution grid of ESB and which is considered for the voltage control

Since the frequency control techniques developed in WP2 consider only devices in the HV and MV grids and the voltage control techniques developed in WP3 control devices in the LV grid, the simulation studies are divided into two cases which are depicted in Figure 2.1.

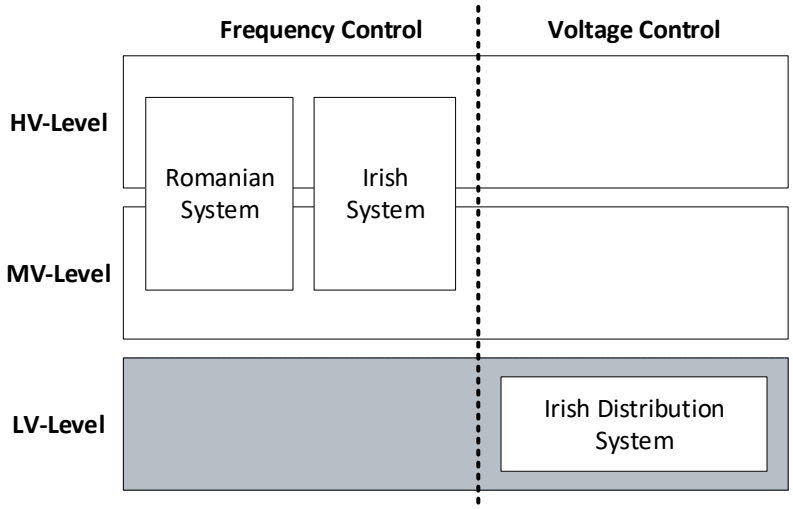

Figure 2.1: Overview of the grid sections considered for frequency and voltage control studies

2.1 High Voltage Level

Two grids are considered for the HV level: a grid derived from the Romanian transmission system and a grid derived from the Irish transmission system. While the Romanian system is representative for many European countries, the Irish system is particularly interesting for frequency control in low-inertia system due to its decoupling from the European mainland grid. Being interconnected through AC tie lines with other neighboring countries allows to take advantage of the inertia of neighboring countries. Ireland, on the other hand, has only two HVDC connections with UK. Hence, Ireland cannot rely on other countries when it comes to overcoming any low-inertia-related issue.

2.1.1 Romanian System

The HV system investigated in Task 5.4 is derived from the Romanian transmission system. The Romanian power system consists of:

- 81 substations, including one 750 kV substation, 38 substations at 400 kV, and 42 substations at 220 kV, as well as 216 transformers with a total installed power of 38,058 MVA.
- 8,834.4 km of transmission lines encompassing 3 km of 750 kV lines, 4915 km of 400 kV lines, 3875.6 km of 220 kV lines, and 40.4 km of 110 kV lines, of which 486.2 km are interconnection lines.

The HV system used in the RESERVE project considers only the HV buses and lines of the Romanian transmission system. The full model of the Romanian power system database contains

about 1500 nodes. Therefore, all the 220 kV and 110 kV elements are aggregated to the 400 kV nodes.

Figure 2.2 shows the geographic location of the main (groups of) power plants in Romania, where the different types of generation are represented in different colors. Additional spots illustrating the presence of small generation units can be added, but they are not of interest for our simulations because load and generation are balanced locally. As can be seen, the largest share of generation is concentrated in the south and so are the transmission lines.

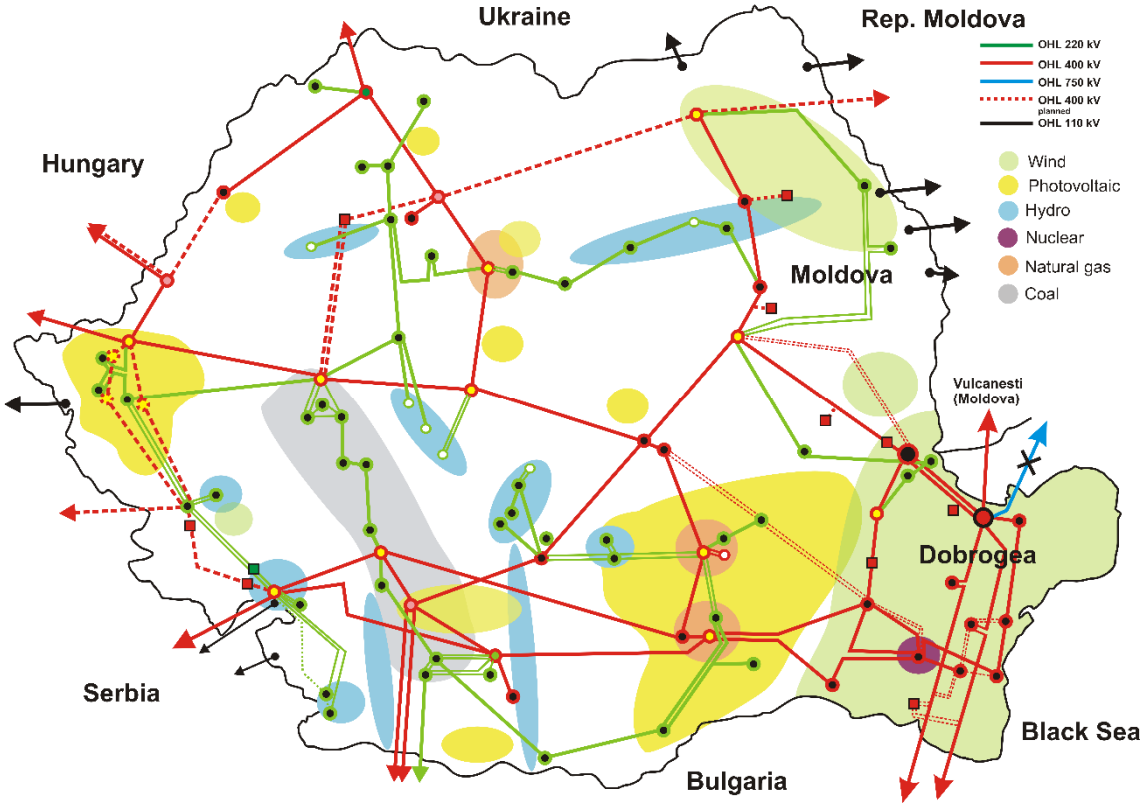

Figure 2.2: Single-line diagram of the Romanian transmission grid and geographic location of the generation sources [2]

Some observations can be made about the geographic location of the power plants:

- The **coal**-fired power plants are located in the same area, as indicated by the gray color.
- Few large **gas**-fired power plants, running all year, are located in two positions. During winter, city power plants are used to produce combined heat and power.
- The **hydraulic** power plants are spread in a large area, and the generation is shared between run-of-river and storage-dam power plants in balanced proportion.
- Out of the 3025 MW [1] installed **wind** capacities in Romania, about 86% (about 2600 MW) are in the Dobrogea region, near the Black Sea. The rest of 14% is mostly located in the North-East of the country.
- A 2x700 MW **nuclear** power plant is also located in Dobrogea, thus more than 4000 MW of installed power are concentrated in this region.
- **Photovoltaic** power plants are spread all over the country; however, the largest power share is located in the south of the country.

Figure 2.3 depicts the development of energy generation since 2008. It can be seen that the power generation from coal and natural gas has decreased from ~55% to ~39%. Meanwhile, the generation from renewable energy sources has increased from ~28% in hydro generation to ~44% since wind and solar are contributing with ~15%.

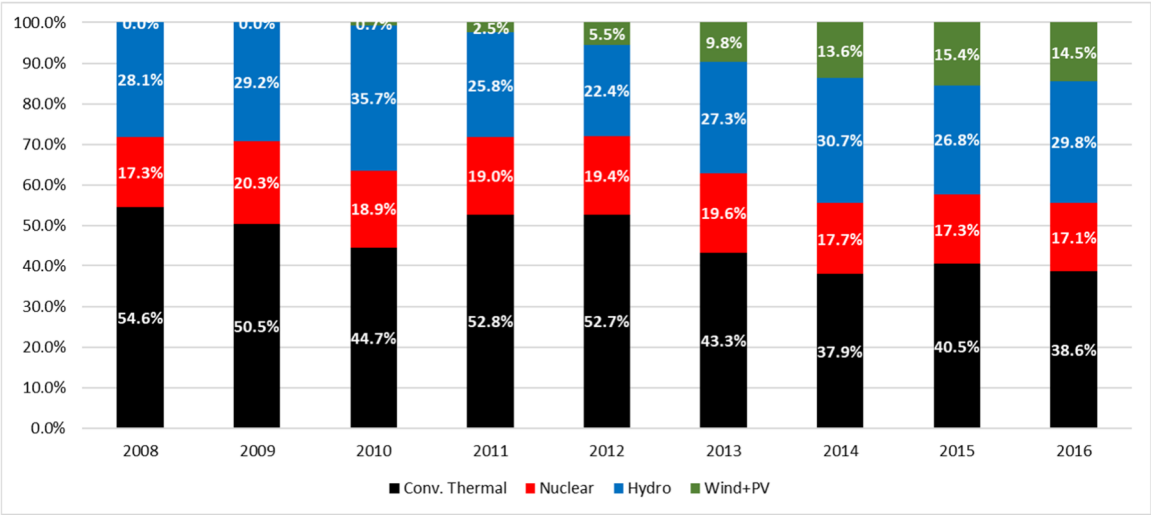

Figure 2.3: Share of electrical energy generation in Romania [3]

According to Transelectrica [4], in 2015, the demand for approval of new wind power plants was about 4550 MW in Dobrogea only. Furthermore, there are requests for approval of new wind power plants in the Moldova region of Romania. All these projects are in stand-by, while no wind power plant was commissioned in 2017 because of the change in the legislation for supporting renewable energy sources by green certificates.

The coal- and gas-fired power plants, most of them located in the south, will be replaced with RES based power plants, also located in the south. The transmission network may not require dramatic changes in the configuration, however, new transmission lines may be required to relay the power produced in Dobrogea region. It is foreseen that construction of new AC transmission lines is more and more difficult because of the cost of the land, and therefore, HVDC technology will be adopted.

Based on the above-mentioned assumptions, three network configurations of the Romanian power system have been considered for the 2030 time horizon:

- RO-195 bus system, that includes the whole 400kV transmission network, and the block transformers of the power plants;
- RO-119 bus system, reduced to the southern part of the transmission network;
- RO-29 bus system, reduced to the Dobrogea region; the reason for keeping this region is that in the future, the largest part of the generation capacity will be installed here.

2.1.2 Irish System

A detailed transient-stability model of the All-Island Irish Transmission System (AIITS) is utilized in the simulations and case studies discussed in Section 5 of this deliverable. The system is characterized by a high penetration of wind power plants (up to 70% in some periods), a relatively small peak of demand (about 6 GW), and it is not synchronously connected to any other grid (only two HVDC connections to UK). These features make the AIITS an excellent test-bed to study the frequency estimation techniques and the Rate of Change of Frequency (RoCoF) and fast frequency control strategies proposed in Deliverable D2.1 and discussed in Chapter 3 of Deliverables D2.6 and D2.7.

The topology and the static data of the system are available at the webpage of the EirGrid Group, the Irish TSO. Dynamic data have been guessed based on the technologies and the capacities of conventional and renewable power plants. Hence, although they are realistic, simulation results do not represent any operating condition of the actual Irish grid.

The system consists of 1,479 buses, 1,851 transmission lines and transformers, 245 loads, 22 conventional power plants modelled with 6th order synchronous machine models with Automatic Voltage Regulations (AVRs) and Turbine Governors (TGs), six Power System Stabilizers (PSSs), and 176 wind power plants, of which 142 are equipped with Doubly-Fed Induction Generators

(DFIGs) and 34 with Constant-Speed Wind Turbines (CSWTs). A map of the AIITS is shown in Figure 2.4 [6].

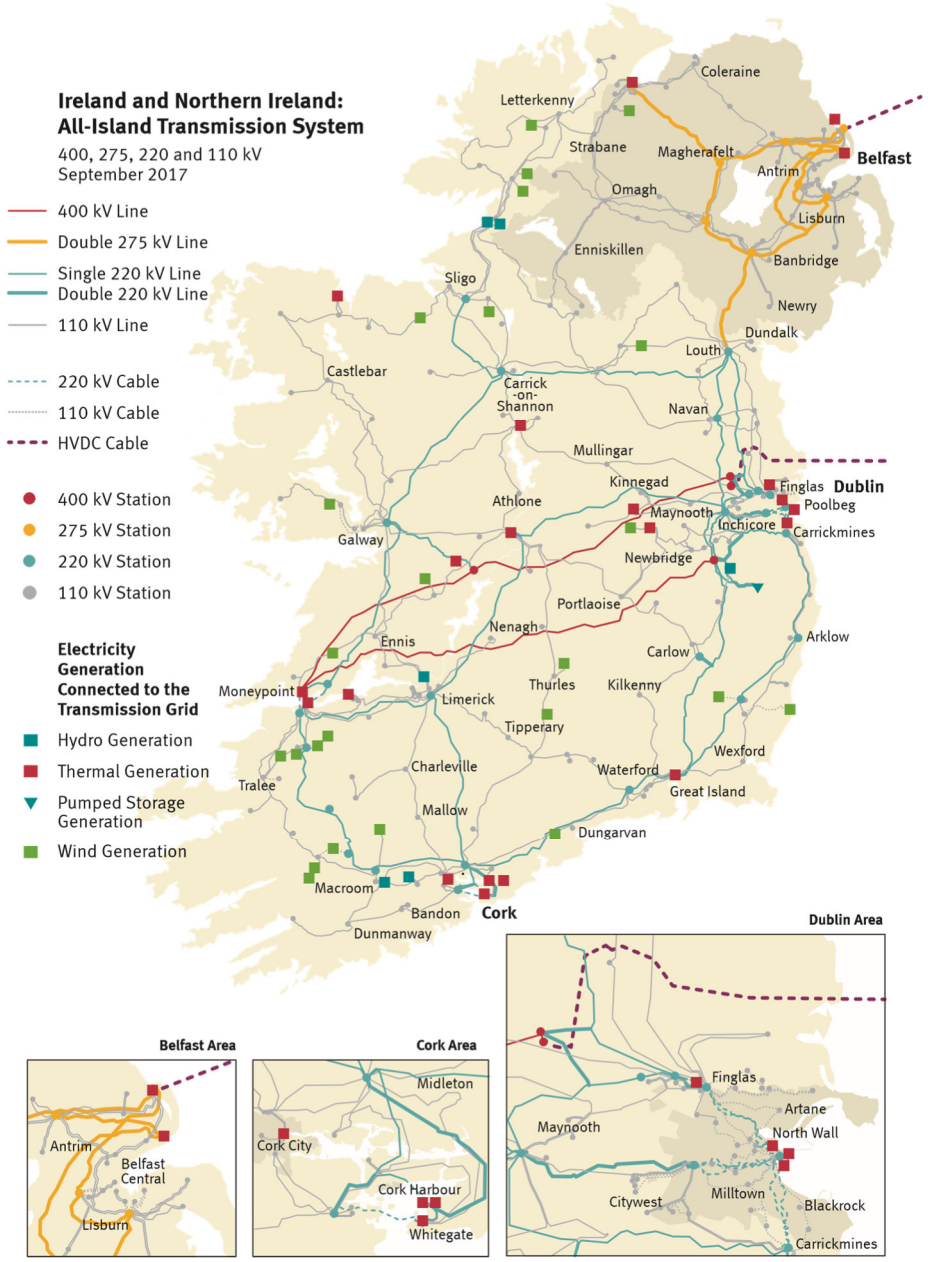

Figure 2.4: Map of the All-Island Irish Transmission System

2.2 Low Voltage System

The LV feeder for voltage control studies is derived from Irish grid data provided by ESB. Busses 1 to 11 are connected via three phase lines whereas the remaining 9 busses only have single phase connections. This section is connected to the MV grid through a 10kV-400V transformer operating on a fixed tap. Different load profiles are considered for each bus and phase. The single phase representation of the grid is depicted in Figure 2.5.

For the voltage control studies, it is assumed that the 9 buses with single phase connections host a 3kW Vehicle-to-Grid device. The converter of this device has a wireless connection to an edge computing unit running the voltage control algorithm.

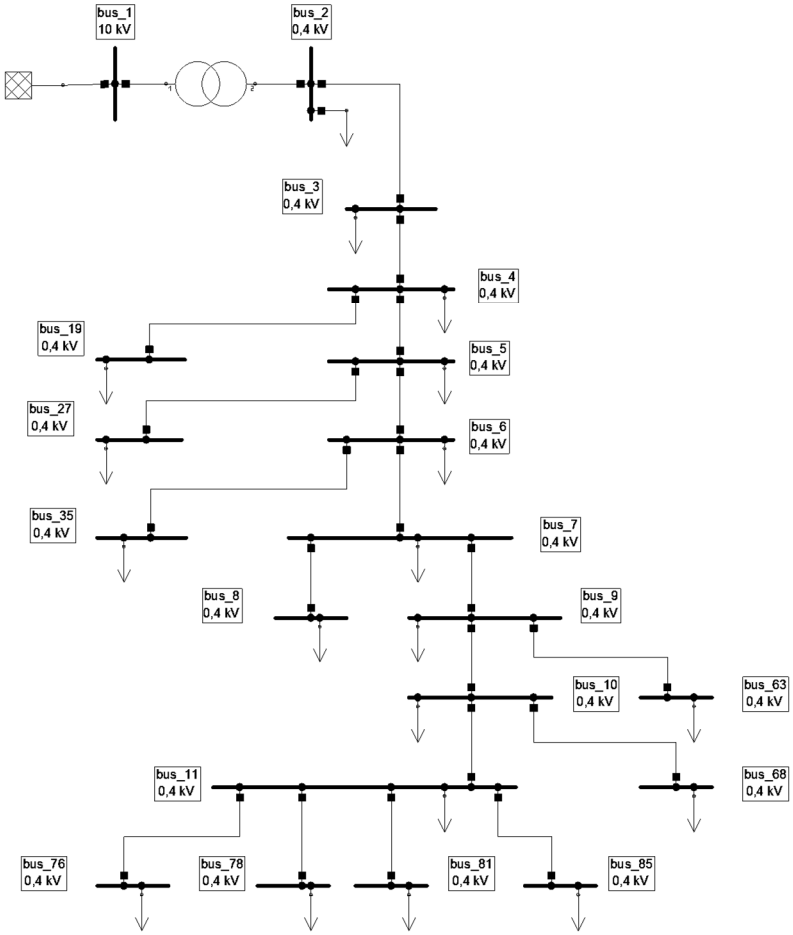

Figure 2.5: LV network feeder

3. Frequency Control Simulation Studies

This section presents the results obtained from simulation studies in the HV system extended with MV level components where the focus is on advanced frequency control techniques. The simulations of the first subsection are based on the synchronously isolated Irish, whereas the second subsection features simulations of the Romanian system that is more representative for European countries.

3.1 Irish System Simulation

This section presents a selection of the simulation results obtained considering the 1,479-bus dynamic model of the all-island Irish transmission system, and that partly substantiate the recommendations for Network Codes and Ancillary Services discussed in Chapter 3 of D2.7. Simulations were carried out in the UCD-based simulation platform Dome [14].

3.1.1 Frequency Maker and Frequency Takers

This section collects the simulation results of the case study that investigates the technical viability of the *frequency maker index* discussed in Chapter 3 of Deliverables D2.6 and D2.7. This index, which is based on the concept of Rate of Change of Power (RoCoP), is aimed at discriminating between frequency makers versus frequency takers. This approach allows identifying those devices and subsystems that have relevant impact on local frequency variations and, thus, are susceptible to take part in the inertial response, as well as in RoCoF and primary frequency control of power systems. In particular, applications of the RoCoP include (i) the estimation of local bus frequencies and Synchronous Machine (SM) rotor speeds; (ii) the estimation of the inertia of SMs as well as the equivalent inertia of non-synchronous devices coupled to fast Primary Frequency Control (PFC); (iii) an empirical criterion to differentiate between *frequency makers*, i.e. devices that have an impact on the frequency at the point of connection based on sufficiently fast and large variations of its active power injection, and *frequency takers*, i.e. devices that do not have impact at the local frequency either because they have constant or null power injection, or because such a power shows slow and small variations); and (iv) the estimation of the power allocated by a device to regulate the frequency.

3.1.1.1 Case Study Description

The case study considers a section of the AIITS that includes a synchronous machine, four wind power plants, and four loads. The scheme of this subsystem and its connection with the main grid is depicted in Figure 3.1.

The description of the devices connected to buses A through E are as follows.

- Bus A – Synchronous machine of 55 MW capacity and 16.282 kWs/kVA starting time.
- Bus B – Doubly-Fed Induction Generator (DFIG)-based wind power plant generating 23 MW at initial conditions.
- Bus C – DFIG-based wind power plant generating 23 MW at initial conditions coupled to fast frequency control.
- Bus D – DFIG-based wind power plant generating 3 MW at initial conditions.
- Bus E – One Constant-Speed Wind Turbine (CSWT) generating 0.25 MW at initial conditions.

All wind power plants follow stochastic wind perturbations. Different wind profiles that follow exponentially auto correlated Weibull-distributed processes are modelled. The set of stochastic differential equations that model the stochastic processes can be found in [7], whereas the parameters used to generate the wind profiles have been obtained from [8].

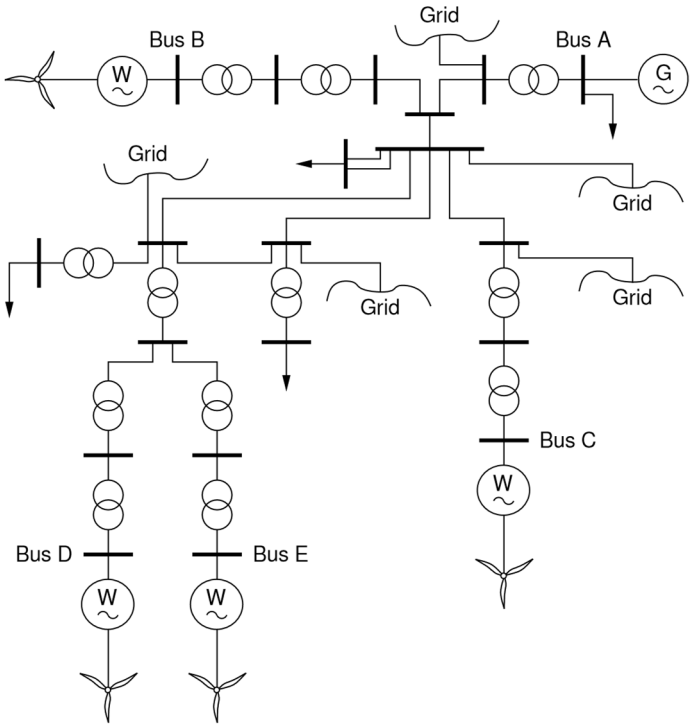

Figure 3.1: Section of the AIITS

3.1.1.2 Simulation Results

Figure 3.2 shows the estimation of the RoCoP for the wind plants connected to buses B, C and D. In this study, 1,000 trajectories of 120 s of duration have been generated with different wind profiles, and no fast frequency control is implemented in any wind plant. The left panel shows the histograms of the trajectories at the end of the simulations, whereas the right panel shows the probability density function (PDF)-fit of each histogram to a normal distribution with mean $\mu_{\dot{p}_B,i} = 0\ \mathrm{pu(MW)/s}$ and standard deviations:

$$\sigma_{\dot{p}_B,B} = 2.18 \cdot 10^{-3}\ \mathrm{pu(MW)/s}$$
$$\sigma_{\dot{p}_B,C} = 3.14 \cdot 10^{-3}\ \mathrm{pu(MW)/s}$$
$$\sigma_{\dot{p}_B,D} = 4.24 \cdot 10^{-4}\ \mathrm{pu(MW)/s}$$

As expected, wind plants with larger capacities lead to higher values of $\sigma_{\dot{p}_B,i}$. The wind plant at bus D shows a $\sigma_{\dot{p}_B,i}$ that is about an order of magnitude smaller than that of buses B and C. For this reason, the CSWT connected to bus E has been omitted in this comparison. Less expectedly, $\sigma_{\dot{p}_B,i}$ shows non-negligible differences (about 30%) between wind plants of same technology and capacity such as those of buses B and C.

The different behavior of the wind power plants is due to various factors. These include:

1. How the plant is connected to the main grid (topological reasons);

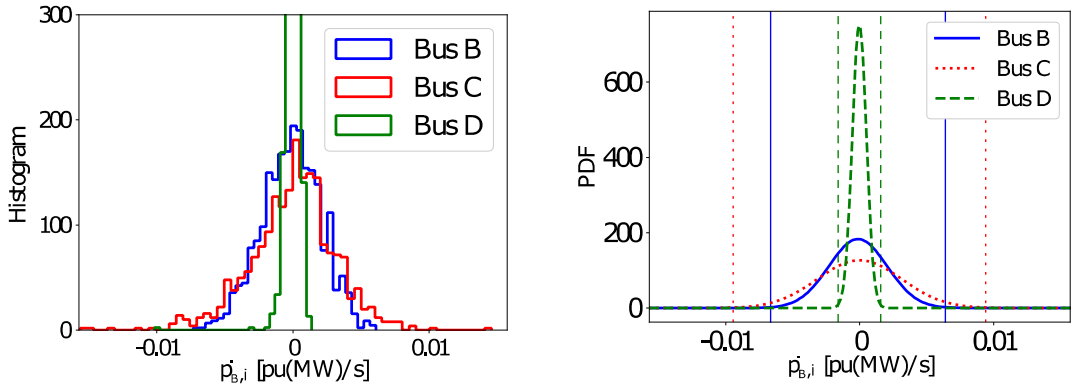

Figure 3.2: Histogram and PDF of the RoCoP at buses B, C and D for 1,000 trajectories. Fast frequency control is not included in the wind plants. The vertical lines indicate the value of $\pm 3\sigma_{\dot{p}_{B,i}}$.

2. the location of the plant and the typical wind profile that is characteristic of that location (geographical reasons); and
3. the number of wind turbines in operation within the plant in the considered time period (technical reasons).

Figure 3.3 shows the PDF-fit of the RoCoP at buses B, C and D when fast frequency control is implemented in the wind plant at bus C. The wind variations are not large enough to trigger the control. Thus, $\sigma_{\dot{p}_{B,C}}$ shows a similar value as for the case without control: $\sigma_{\dot{p}_{B,C}} = 3.29 \cdot 10^{-3}$ pu(MW)/s.

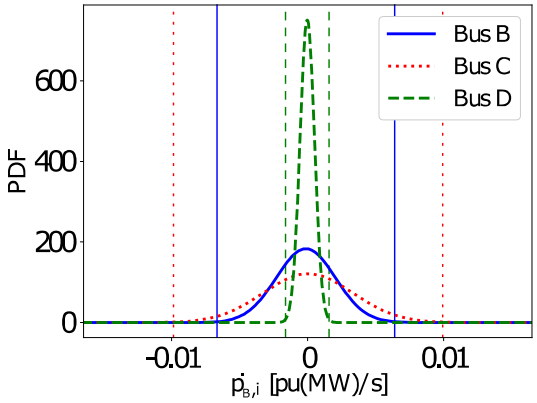

Figure 3.3: PDF of the RoCoP at buses B, C and D for 1,000 trajectories. Fast frequency control is included in the wind plant at bus C. The vertical lines indicate the value of $\pm 3\sigma_{\dot{p}_{B,i}}$.

Figure 3.4 shows the trajectories of the RoCoP at buses B, C and D (left panel), and the variations of the active power injected and equivalent *inertial* power at buses B and C (right panel) for a single trajectory with stochastic wind perturbations and fast frequency control implemented at bus C.

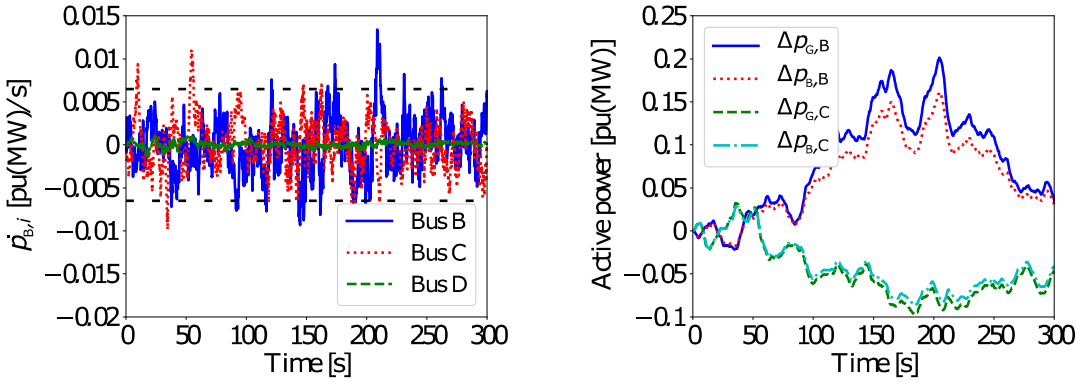

Figure 3.4: Trajectories of the RoCoP at buses B, C and D; and variations of the active power injected and equivalent 'inertial' power at buses B and C. Fast frequency control is included in the wind plant at bus C.

Let us define the threshold $\epsilon_{WT} = 3\sigma_{\dot{p}_{B,B}} \approx 6.5 \cdot 10^{-3}$ pu(MW)/s, marked with horizontal dashed lines in the left panel of Figure 3.4. We can thus safely determine that the wind power plant at bus D is a *frequency taker*. For this reason, the plant at bus D (and consequently, the plant at bus E), are not considered in the remainder of this study.

The indexes of buses B and C are, for most of the time, within the thresholds $\pm\epsilon_{WT}$. On the other hand, if only the measures of the variations of the active power injected by the wind plant (or the estimation of its equivalent inertial power as shown in the right panel of Figure 3.4) are available, intuitively one can assume that the plant at bus B without frequency control will have, *a priori*, a greater impact on its local frequency than that at bus C with control, as opposed to the results obtained from Figure 3.3.

This is illustrated in Figure 3.5, where the loss of a 44 MW, 13.2 MVAr load is simulated at $t = 50s$. The RoCoP index clearly indicates that the wind power plant is providing frequency control as observed from the values of the index in the few seconds after the contingency. This is not so clear from the active power injection shown in the right panel of the figure. After $t = 50s$, the index shows a ramp that, in magnitude, is even smaller than other ramps observed from bus C (see e.g. the variations in $t \in [160,220]s$).

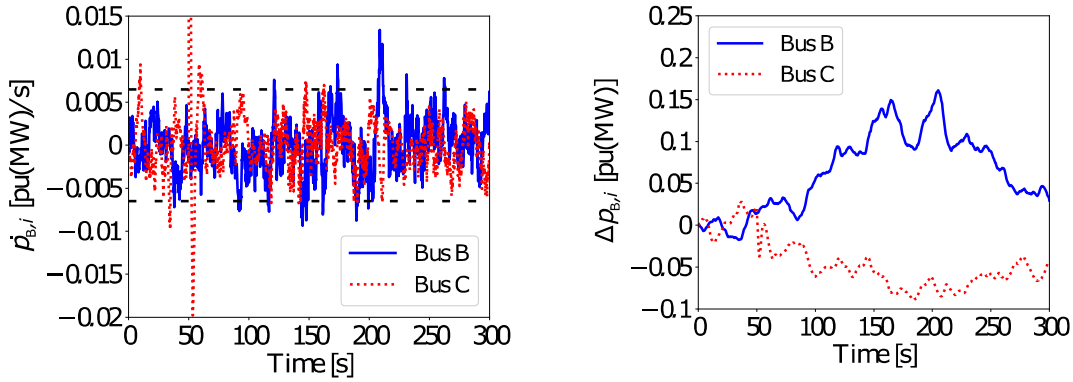

Figure 3.5 Trajectories of the RoCoP and estimated equivalent 'inertial' power at buses B and C following a loss of load. Fast frequency control is included in the wind plant at bus C.

3.1.2 Fast Frequency Control and Stability from Converter-Interfaced Energy Storage Systems in Transmission Systems

For the purpose of this case study, a hybrid CI-ESS (HESS) composed of a Flywheel ESS (FESS) and a Battery ESS (BESS) is installed in the AIITS. Different stochastic processes are applied to

the loads, and to the wind for each wind power plant. Two scenarios are shown below. First, fast frequency control provided by the HESS is studied in Section 3.1.2.1, while the capability of the HESS to increase the critical clearing time (CCT) of a fault is demonstrated in Section 3.1.2.2.

3.1.2.1 Fast Frequency Control

In this scenario, the system variable regulated by the HESS is the frequency of the bus at which the storage device is connected to. The contingency considered is the disconnection of one of the synchronous machines of the system that is generating 50 MW prior the contingency. 1,000 simulations are performed for each case, namely with and without HESS, and results are shown in Figure 3.6 and Figure 3.7, where the histograms of the frequency of the bus of connection, ω_{Bus}, as well as its probability density function (PDF) are represented for two conditions, namely at the frequency nadir, and 10 s after the generation unit outage. In the figures, μ_ω represents the mean of the PDF, while σ_ω stands for the standard deviations of the bus frequency.

It can be seen that installing the HESS improves the performance of the system for both the frequency nadir and 10 seconds after the machine outage, as μ_ω is closer to 1 pu (i.e., 50 Hz), and σ_ω is closer to zero, which implies smaller frequency deviations with respect to the mean. A detailed description of the methodology and case study considered in this analysis is provided in [9].

3.1.2.2 Transient Stability

In this scenario, the area where the ESS (either FESS or BESS) is installed includes a synchronous machine that provides 139 MW and 15 MVAr as well as several wind power plants and loads. The controllers of both FESS and BESS can be designed to regulate the frequency of the bus of connection (ω_{Bus}) or the frequency of the center of inertia (ω_{Col}). For the sake of comparison, the analysis also considers a 100 MVar STATCOM device which provides exclusively reactive power regulation [10]. Apart from the stochastic variations of the wind speeds, random initial loading levels have been considered to account for load uncertainty. Same control parameters have been chosen for the reactive power control of the ESS and the STATCOM.

The analysis is based on the results of stochastic time domain simulations (1,000 simulations per scenario, 60 scenarios). The contingency is a three-phase fault, and two different locations of the fault are considered in order to represent two possible system topologies according to the relative position of the fault and the ESS with respect to the synchronous machine, as depicted in Figure 3.8. The percentage of simulations that are unstable due to the loss of synchronism of the machine is then computed for different clearing times (CTs), and shown in Table 3.1 and Table 3.2, for each of the following scenarios:

- Irish system without ESSs.
- One FESS/BESS providing local ω_{Bus} control.
- One FESS/BESS providing ω_{CoI} control.
- One STATCOM device providing local bus voltage (v_{ac}) control.

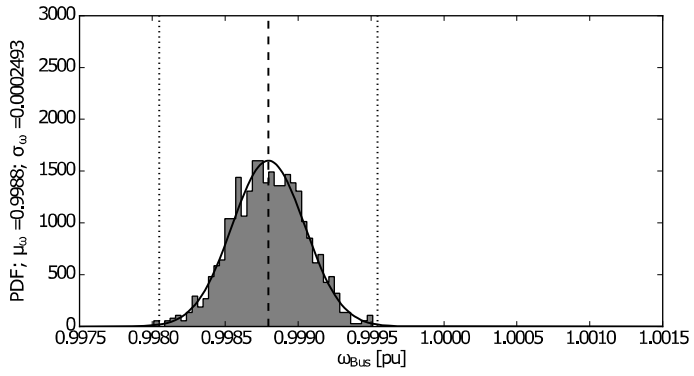

(a) Frequency nadir

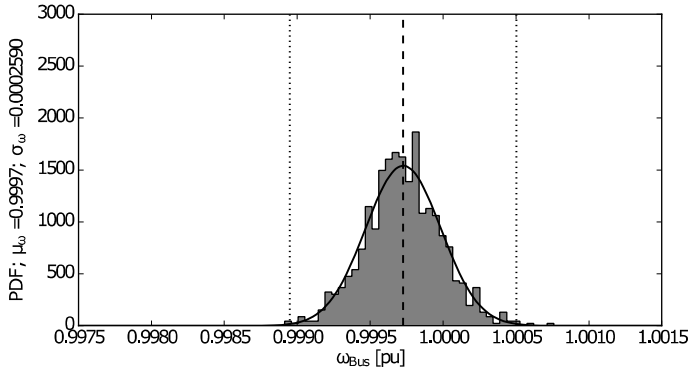

(b) 10 s after contingency

Figure 3.6: AllTS without HESS facing the outage of a generating unit. Dashed line: μ_{ω}; dotted lines: $\mu_{\omega} \pm 3\sigma_{\omega}$.

The concluding remarks from this study are summarized below.

- The reactive power support of the ESS plays the major role in transient stability enhancement.
- Regulating the frequency of the CoI provides fairly similar results than controlling a local bus frequency.
- If the fault occurs between the synchronous machine and the ESS, the support provided by the latter is substantially diminished.
- The STATCOM device outperforms the ESS in some scenarios.

Should the reader desire a more detailed description of the methodology, we refer to [11].

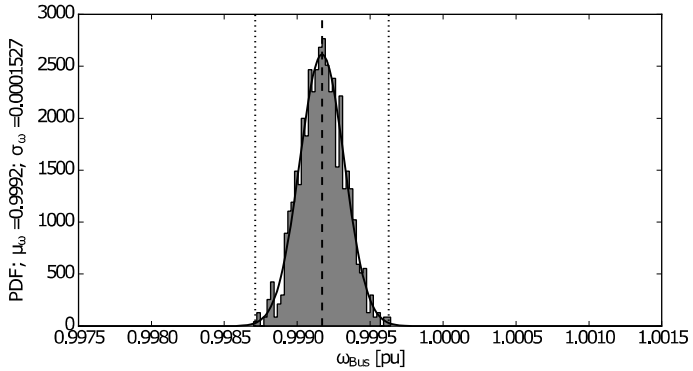

(a) Frequency nadir

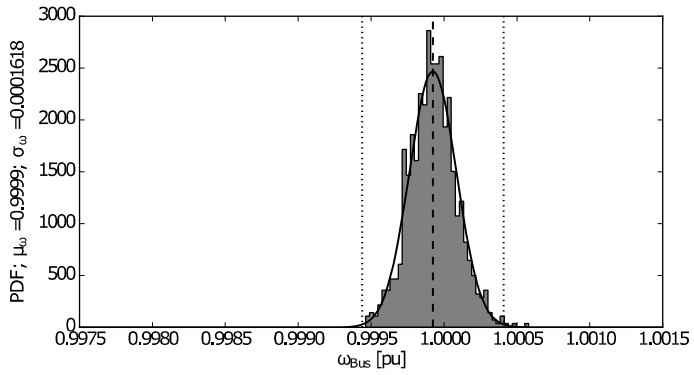

(b) 10 s after contingency

Figure 3.7: AllTS with HESS facing the outage of a generating unit. Dashed line: μ_{ω}; dotted lines: $\mu_{\omega} \pm 3\sigma_{\omega}$.

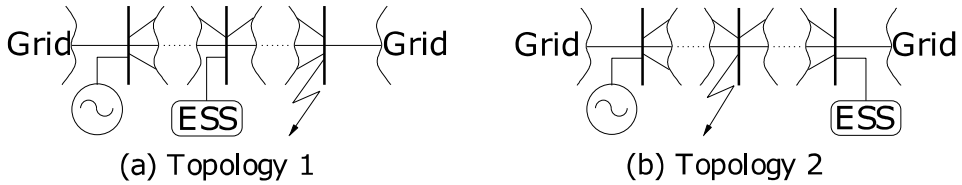

Figure 3.8: Topologies of a power system facing a fault. (a) Topology 1: The ESS and the synchronous machines are on the same side with respect to the fault; (b) Topology 2: The fault occurs between the synchronous machine and the ESS.

Table 3.1: Percentage of unstable simulations after a three-phase fault for Topology 1 in the Irish system for different clearing times (CT).

CT [ms]	105	110	115	120	125
No ESS	25.3	44.4	65.6	83.1	99.9
ω_{bus} Control					
FES	3.0	26.2	46.5	65.0	85.1
BES	8.9	31.8	50.4	71.1	88.0
ω_{Col} Control					
FES	1.5	24.1	43.5	63.6	81.9
BES	2.4	25.4	43.9	64.2	82.1
v_{ac} Control					
STATCOM	5.8	28.9	47.0	67.5	84.7

Table 3.2: Percentage of unstable simulations after a three-phase fault for Topology 2 in the Irish system for different CTs.

CT [ms]	105	110	115	120	125
No ESS	29.8	48.7	69.4	86.5	100.0

ω_{bus} Control					
FES	19.2	41.0	57.0	80.2	97.7
BES	22.9	43.3	62.4	81.8	100.0
ω_{COI} Control					
FES	17.5	39.7	58.2	78.1	96.2
BES	17.8	39.8	59.1	78.2	96.6
v_{ac} Control					
STATCOM	16.7	39.1	57.4	76.9	95.5

3.2 Romanian System Simulation

The simulations conducted with the Romanian systems have two objectives. As for the Irish system, it is evaluated how a large share of renewables could be supported by integrating them in frequency control techniques. Furthermore, simulations on the complete Romanian data set should demonstrate the real-time capability of the dynamic phasor simulator DPsim [12] developed in the RESERVE project.

Apart from splitting up networks and distributing the computational load by distributing the simulation model parts to several simulation sites, the simulation of larger grids could be enabled by simulating parts of the grid in dynamic phasors. Electromagnetic transient (EMT) simulations are only conducted for the parts which require high accuracy also in dynamic situations. Dynamic phasors do not lead to a degradation of accuracy per se as shown in D4.2. The advantage of dynamic phasor is that the simulation time step can be increased, which leaves more time for computation in each simulation step and the exchange of data between simulation sites.

Since there is no commercial dynamic phasor real-time solver available today, DPsim is developed as a reference simulator within task 4.3. EMT simulations are conducted in commercial EMT solvers as shown in Figure 3.9.

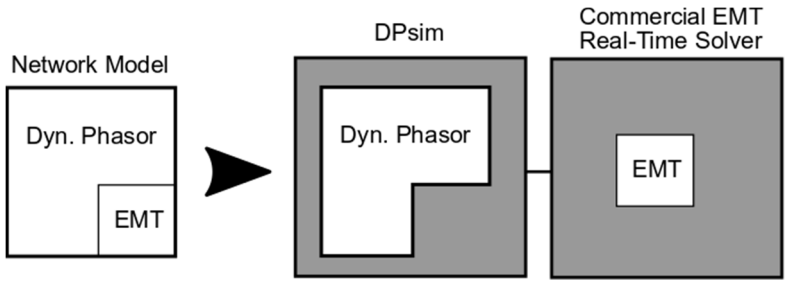

Figure 3.9: Co-simulation using dynamic phasor and EMT

The advantage of this combination of solvers is that Hardware-In-the-Loop experiments, which require a very accurate, small time step simulation, can be conducted in the EMT simulator while the surrounding network is simulated on a broad scale instead of being represented by an aggregated equivalent model or a very detailed EMT model which would be much more demanding in terms of computational power.

3.2.1 Detailed Scenario

Figure 3.10 illustrates the one-line diagram of the Dobrogea region from the Romanian power system. The Dobrogea region was chosen for simulations because it hosts ≈80% of the power installed in wind power plants. Additionally, currently there are two large nuclear units located at Cernavoda (generators represented in yellow), while one more unit is planned to be built here depending on the political decisions.

In order to simulate the power exchanged with the neighboring areas, an external system was considered, consisting of two hydro units (represented in blue) and one load, together with the interconnection lines. Additionally, the interconnection with the Bulgarian power system was

simulated by considering static loads at the ends of the two interconnection lines on the Southern part.

A VPP was created in the Dobrogea area, by considering two active wind power plants (represented in green) at Stupina and Tariverde, modelled by a variable power generation curve. We assume that a VPP can work efficiently by including also one BESS (represented in orange). In our model, we assume that the storage system connected to Stupina bus.

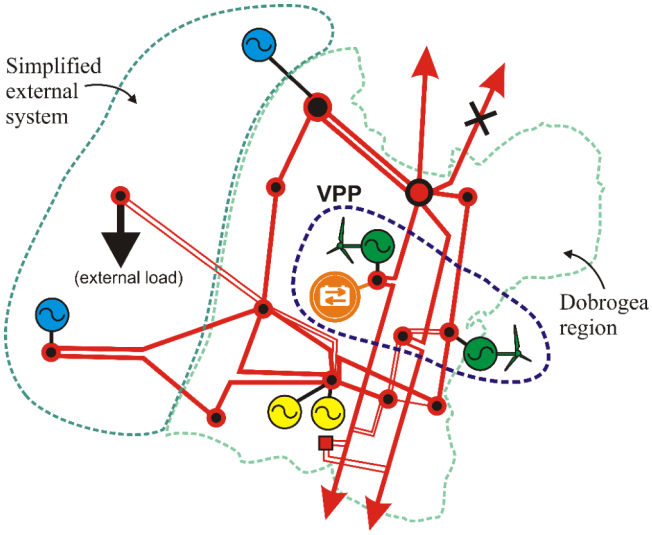

Figure 3.10: The reduced system of Dobrogea

Simulations have been performed in Simulink. The model implemented is illustrated in Figure 3.11. In this scheme, the synchronous machines are colored in red, and the loads are colored in orange. The total simulated in this model is ≈1800 MW.

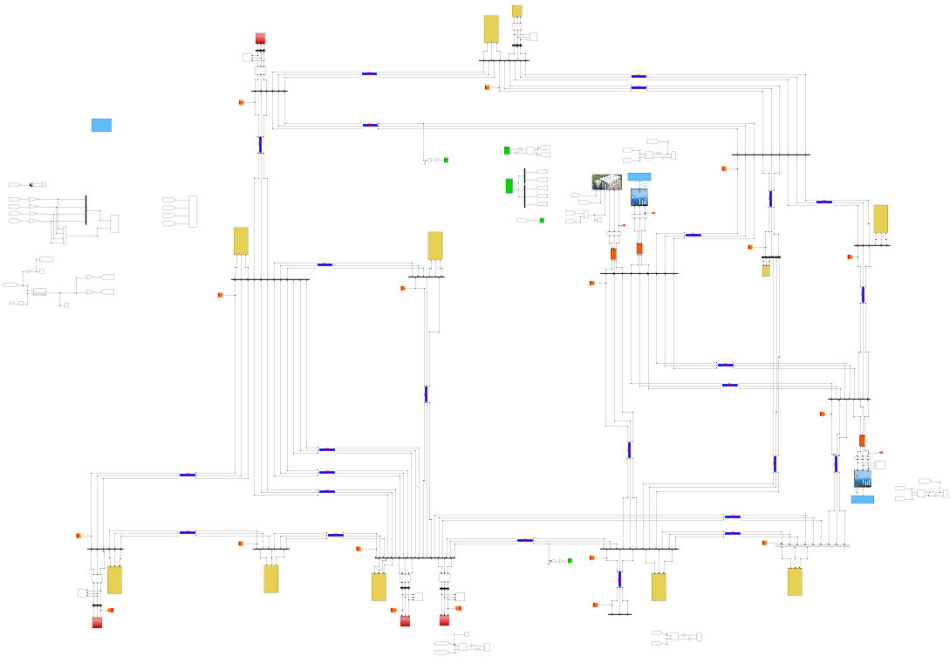

Figure 3.11: The simulated network implemented in Simulink.

In the RESERVE project we support the wide scale development of storage systems, and in particular those interfaced by power electronics for which the inertia is simulated using power electronics control techniques.

The main purposes of these simulations are to demonstrate:

- The operation of a VPP;
- The integration of a BESS into a VPP;
- Integration of a VPP into the frequency restoration control (FRC) system;
- The use of BESS for frequency containment control (FCC).

The modelling and technical details of the controllers are presented in deliverable D2.7.

Scenario A: FRC and VPP control are active

We assume a perturbation consisting of a sudden connection of a 100 MW load, at 30 s from the simulation start. The FRC is activated 30 seconds after the perturbation occurrence. This perturbation is equivalent, in terms of power unbalance, with the disconnection of a 100 MW generator. The simulation is performed with and without FCC.

Figure 3.12 shows the importance of a rapid contribution of a storage system to limit the frequency nadir. In our model, the frequency drops to a dangerous value when synchronous machines only are considered to operate in droop mode. However, in these simulations we have to note that the Dobrogea area is provided with strong mechanical inertia from the nuclear power plants.

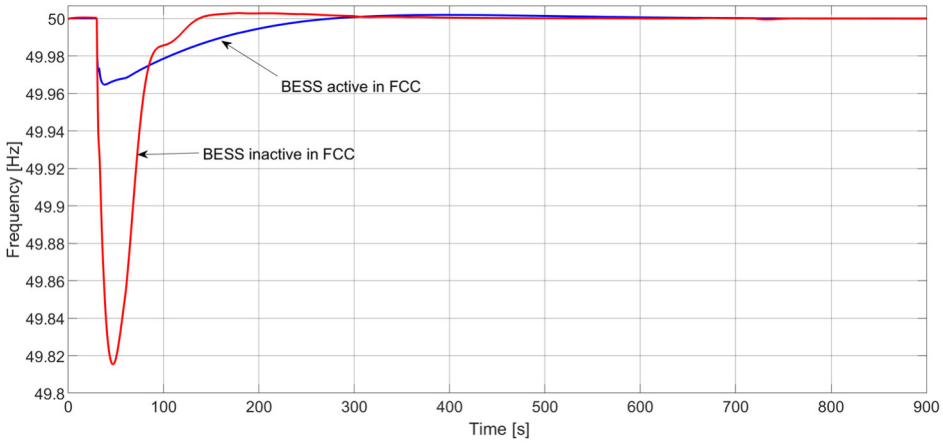

Figure 3.12: Frequency dynamics in the case with and without BESS active in the FCC loop.

The BESS was sized to 50 MW and 60 MWh. The state of charge (SoC) of the BESS is initialized to 50%, assuming that the power variations can be either positive or negative. In our simulations, because of the loss of a large load, the BESS is ordered to produce power.

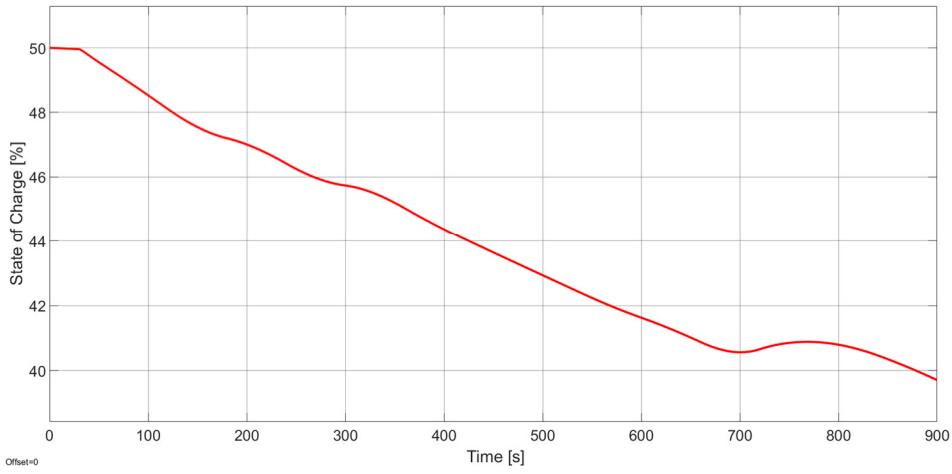

Figure 3.13: State of charge of the BESS in the case with VPP control active.

The BESS controller includes three control signals, one as frequency response in FCC, one as power order from the AGC (or FRC), and one as balancing response within the VPP. Figure 3.14 illustrates the BESS power variations in in the three control loops, as well as total power response. BESS provides power very quickly after the perturbation start then decreases towards zero, while

the AGC power is initiated at instant 60 s and, together with a synchronous machine acts to replace the frequency containment reserve and to bring the frequency close to the reference value.

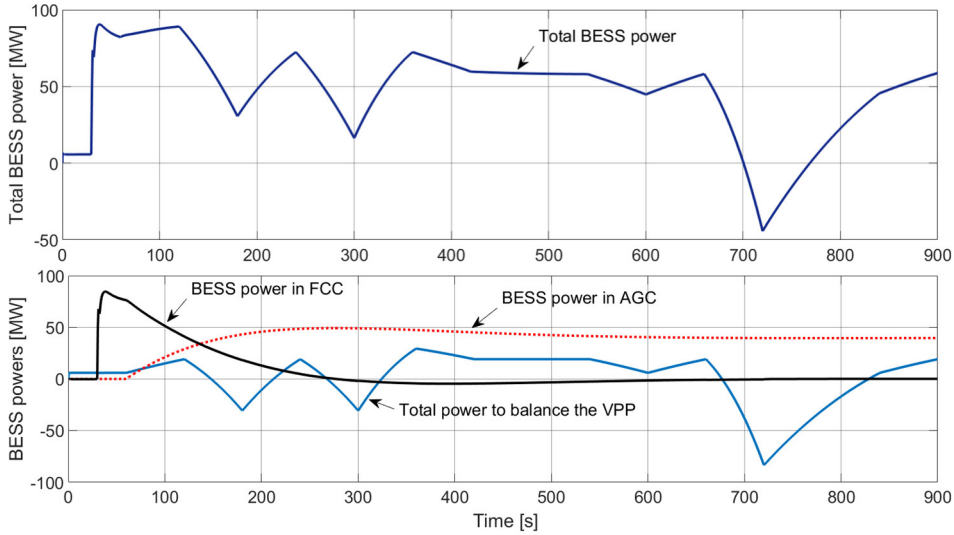

Figure 3.14: BESS control powers.

The VPP is set to produce a constant power. Since the two wind generators are fluctuating, the BESS either produce or absorb power to balance the wind generation and maintain the VPP power at the predefined value. We should note that if the VPP requires negative power, and the AGC required positive power, the total generation is the aggregation of the two.

Scenario B: FCC and FRC are active, and VPP control is inactive

In order to understand the importance of the BESS for VPP balancing, in this scenario we consider that the VPP is not used for VPP control. Figure 3.15 shows that the fluctuations in the wind power generation may have an impact on the frequency. Small frequency variations are experienced because the AGC regulator is too slow, while FCC is not designed to recover the frequency.

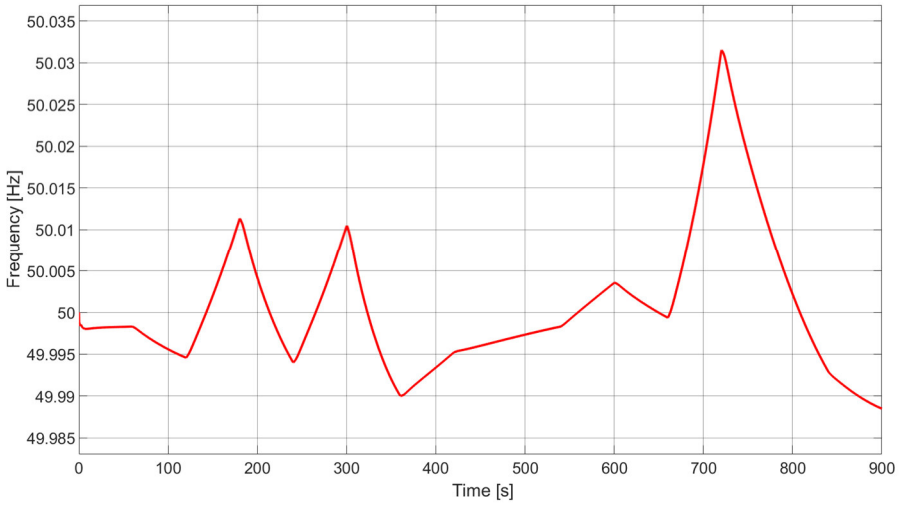

Figure 3.15: Frequency variation in the case when BESS is not active in VPP control.

Figure 3.16 shows the SoC variation caused by the variation of the wind generation. BESS is either charging or discharging depending on the need to control the frequency. As compared to Scenario A, SoC is increasing and decreasing around the middle value. This may show that storage systems are suitable for frequency control, but wrong or inaccurate wind generation forecasts may cause the BESS to exhaust very quickly its energy if not appropriately sized. The

SoC variation in Figure 3.16 is less than 1% because the considered BESS has a very large capacity.

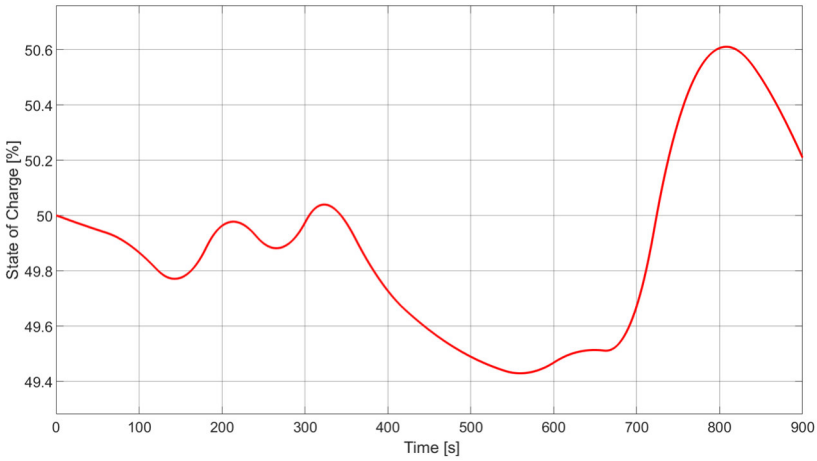

Figure 3.16: State of charge of the BESS in the case without VPP control active.

Concluding remarks:

- Storage systems are essential in power balancing and frequency control;
- VPP concept is a “must” to better balance the intermittent sources;
- Because of the slow response, VPPs can be integrated into the FRC scheme.

3.2.2 Large Scale Scenario

The evaluation of DPsim in a large scale scenario is conducted using two different grids. The Romanian power system with 195 nodes and a synthetized system which is composed of copies of the WSCC 9-bus system.

In the following results it is visible how DPsim performs in two different modes:

- Sequential and
- Parallel execution

For the sequential simulation, all computation steps of component states and the network solution are executed consecutively. A detailed description of the required calculation steps can be found in deliverable D4.2 and D4.3.

In the parallel simulation, all components and if available subsections of the network are solved in parallel as much as possible. Whether the calculations can be executed in parallel is determined by a directed task dependency graph that is determined automatically by DPsim before the simulation start. An example of such a graph is depicted in Figure 3.17 where tasks are represented by circles. The size of the circles represents the computation time of each task and the directed connections show the dependency.

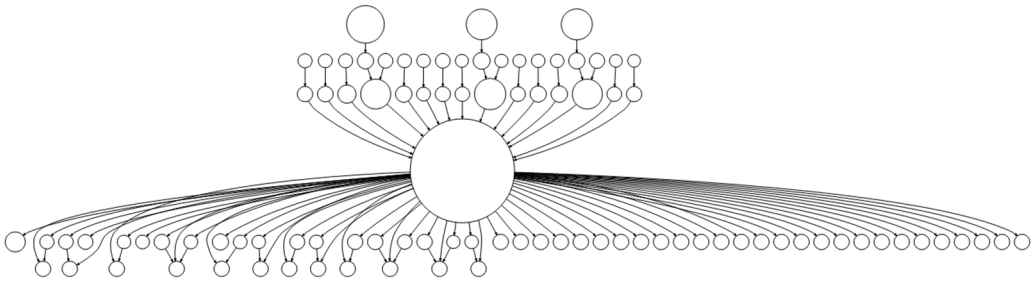

Figure 3.17: Task dependency graph of a DPsim simulation with one network solution

For the Romanian grid data depicted in Figure 3.18, it can be seen that the parallelization has a visible but not significant impact on the average computation time per simulation step. This is because the network system solution is requiring most of the computation time as it is also the case for the task graph presented in Figure 3.17.

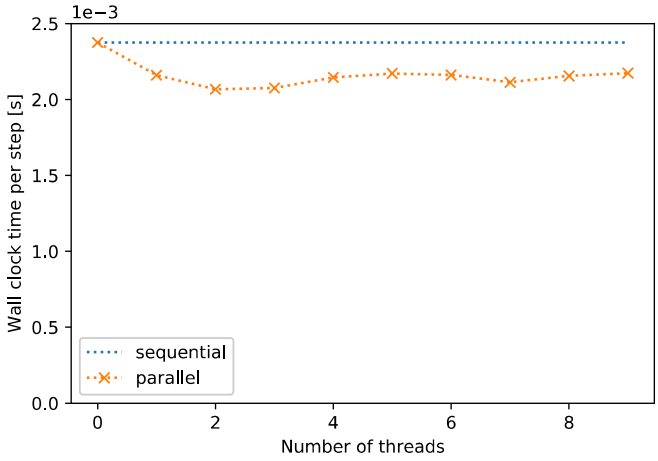

Figure 3.18: Average simulation time step of Romanian power system in DPsim

A solution would be to identify transmission lines that could be used to decouple subsections of the system. In order to investigate the effect of decoupling lines and the system size more systematically, we have created several network models that are composed of copies of the WSCC 9-bus system. The 9-bus systems are coupled as shown in Figure 3.19. Only busses of the same voltage are connected so that no power flow between the systems is expected. The interconnecting lines are created as transmission lines using the Bergeron transmission line model (TLM), which allows to decouple subsection of the network.

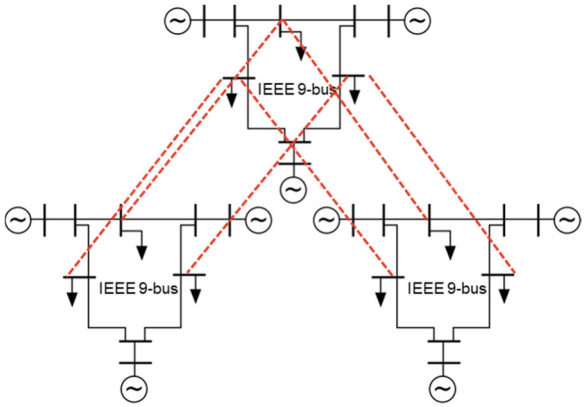

Figure 3.19: Interconnected copies of the WSCC 9-bus system

The simulation results depicted in Figure 3.20 show that the parallel execution leads to a significant improvement of the average time per simulation step. For 40 interconnected copies of the 9-bus system, the time per simulation step is still close to 100 µs compared to more than 10 ms in a sequential simulation. A more detailed discussion on the parallelization can be found in [12].

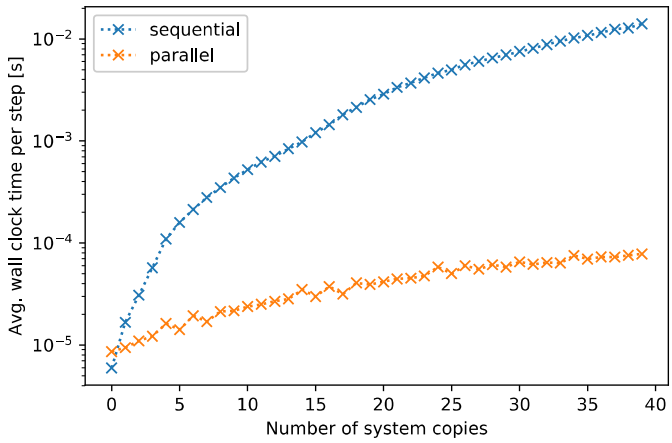

Figure 3.20: Average simulation time step of multiple interconnected WSCC 9-bus systems in DPsim

4. Voltage Control Simulation Studies

Both voltage control concepts, the static and the dynamic, have been evaluated using a real-time simulation setup that includes OPAL-RT® as the real-time simulator.

4.1 Active Voltage Management (AVM)

The proposed active voltage management (AVM), described in D3.1, is designed to be deployed to secondary substations which makes it suitable for execution on distributed cloud systems as represented in blue in Figure 4.1.

The distributed cloud system in a flight rack is located in the RWTH laboratory and includes edge computing capabilities as well as an LTE mobile Base Station which is connected to the mobile Core Network located outside of the laboratory. The real-time power system simulators in the RWTH laboratory are connected to the distributed cloud system via VILLASnode that is described in detail in deliverable D4.1. Since the power system is simulated in real-time, the LTE wireless connection between the base station and the simulators allows to test new monitoring and control concepts with realistic communication characteristics such as the latency between the Base Station executing the control algorithm and the power system components. More information on the simulation infrastructure can be found in [13].

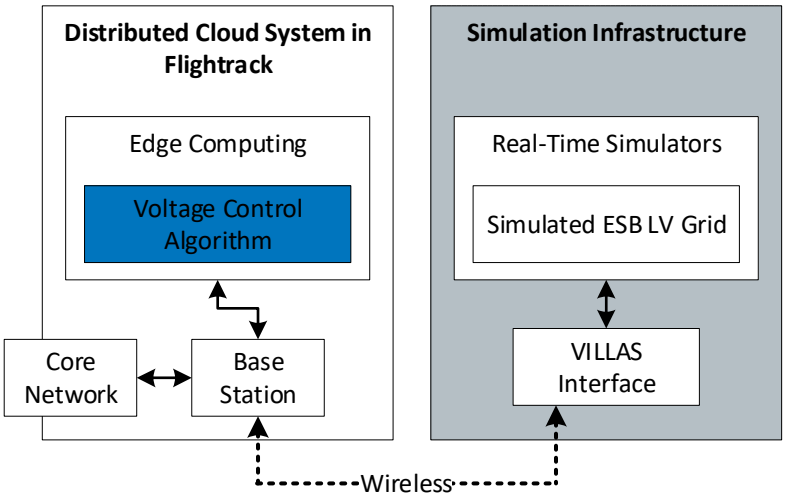

Figure 4.1: Hardware and software components for real-time voltage control experiments

The aim of the voltage control is to reduce the voltage imbalance at the three phase busses of the distribution network. The Irish low voltage network described in Section 2.2 was used for the following simulations. To regulate the voltage, the reactive power output of single-phase connected Vehicle-2-Grid chargers is used. The reactive power is controlled according to the AVM algorithm described in deliverable D3.1.

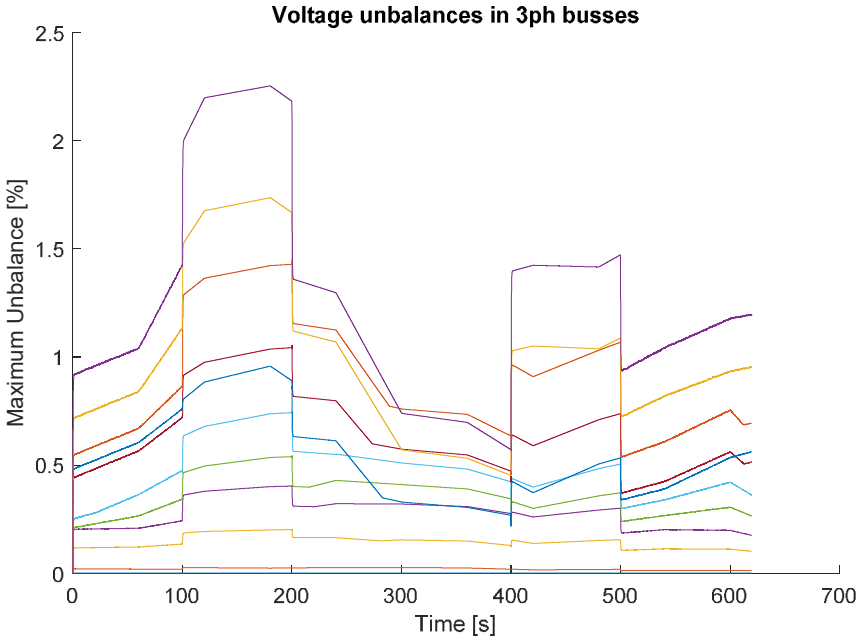

Figure 4.2: Voltage unbalances of three-phase busses with respect to mean bus voltage

During the simulation time that is depicted in Figure 4.2 and Figure 4.3, the voltage is regulated in three time intervals and the control is switched off two times. In Figure 4.2, it is visible how the phase imbalances are reduced at time 200s and 500s when the control is activated again. For the sake of completeness, Figure 4.3 presents the single-phase bus voltages, which are also affected by the control action.

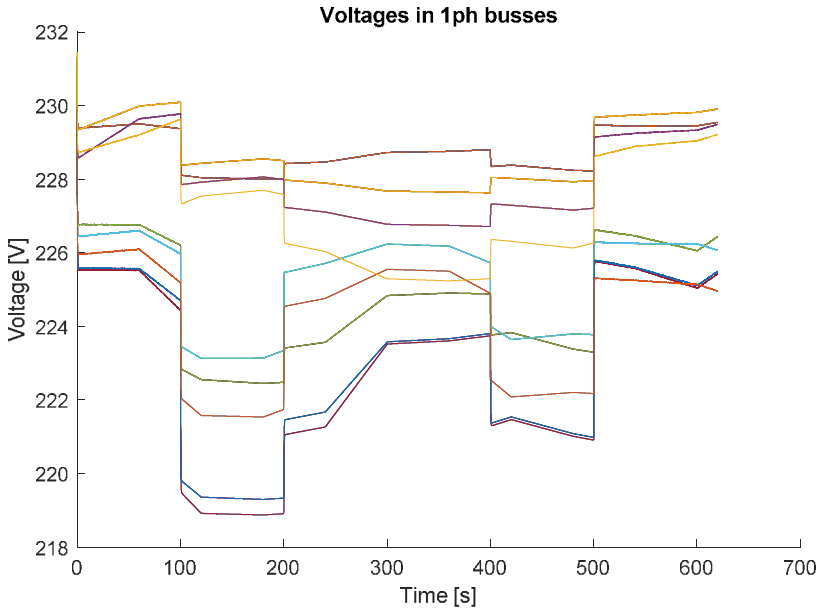

Figure 4.3: Voltages of single-phase buses with V2G chargers

4.2 Virtual Output Impedance (VOI) Control

The simulation consists of a grid-connected converter operating in grid-feeding mode. Unlike all other scenarios such as SF_A, SF_B and SV_B where averaged models of inverters were simulated, SV_B scenario requires switching models of inverter. By averaged model, we mean that the inverter is represented as an ideal sinusoidal voltage / current source and by switched models, we mean that the state of every switch (ON or OFF) in the power-electronic converter is

considered. Thus, switched models cover all the harmonic phenomenon since they are detailed and can enable to understand short-time dynamic situations as dealt by SV_A.

4.2.1 RT-Simulation Description

Table 4.1 presents the parameters of the three-phase grid connected inverter. The table includes operational parameters, filter parameters and control parameters. The grid connected inverter has an LCL output filter with no physical damping or passive damping filter as shown in Figure 4.4.

Table 4.1 Inverter Parameters

Converter Parameters	Values
DC Link Voltage	1000 V
Grid Voltage and Frequency	400 V, 50 Hz
Switching Frequency	5 kHz
Converter Side Choke	3.8 mH, 0.1Ω
Grid Side Choke	3.8 mH, 0.1Ω
Filter Capacitance Co	19.8 μF
Control Parameters (Kp, Ki)	1.832E-4, 1.832

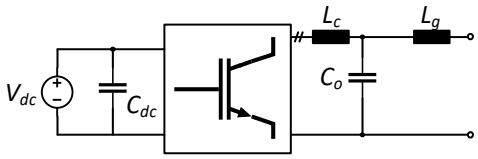

Figure 4.4 Grid connected inverter with LCL Filter

The grid impedance connected to the output of the inverter is shown in Figure 4.5. This impedance is fixed in such a way that it introduces a resonance within the control bandwidth of the inverter.

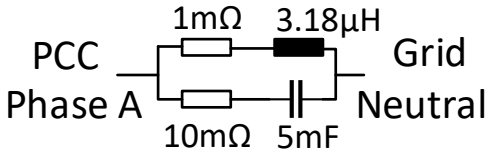

Figure 4.5 Grid Impedance

The VOI controller is designed to emulate the behavior of a passive shunt RC damper. The filter structure of a shunt RC damper is shown in Figure 4.6.

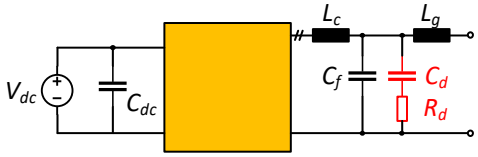

Figure 4.6 Passive damping filter structure to be emulated by VOI controller

Comparing Figure 4.4 and Figure 4.6, the overall capacitance C_o is split into capacitances C_f and C_d. For simplicity, the split ratio can be half, which means $C_d = C_f = C_o/2$. By calculating the characteristic impedance of the LCL filter and choosing an optimal quality factor, the damping resistor R_d can be calculated. For a split ratio of half, the optimal quality factor is 9. The VOI control structure that actively emulates the passive damping structure in Figure 4.6 is given by the following equation.

$$K_{voi} = K_d . \frac{s}{s + \frac{1}{R_d C_d}}$$

Here R_d and C_d refers to the damping resistance and capacitance respectively. By considering an optimal quality factor of 9, the damping resistance R_d is calculated as 88.14 Ω. The control gain K_d is fixed as 0.2. The frequency domain response of the resulting VOI controller is shown in Figure 4.7.

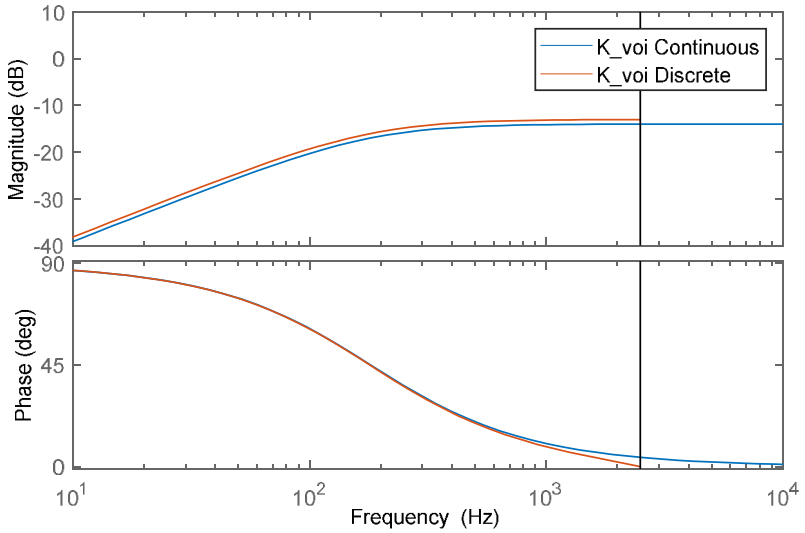

Figure 4.7 VOI Controller in Frequency Domain

Thus, as explained in D3.5, we have two controllers, one PI controller with grid voltage feedforward taking care of output current reference tracking while the other is the VOI controller, which reshapes the output impedance for improving dynamic stability and reducing harmonic distortions.

4.2.2 RT-Simulation Results

The real-time simulation is run at a time step of 10 µs, without any overruns which means the solver can solve the power system within the specified time step of 10 µs. As mentioned earlier, the chosen grid impedance for this converter introduces harmonic instability. Hence, the simulation is started under the presence of VOI. The control parameters are designed by discretizing the system transfer functions at 5 kHz of sampling frequency and a discrete domain PLL is designed by considering a settling time of 30 ms and damping ratio of 0.7 which leads to a highly stable PLL design.

At time $t = 0.3$ seconds, the VOI controller is disengaged and only the output reference tracking controller is active. Thus, the virtual damping provided by the VOI controller is not available. It can be noted from $t = 0.3s$ onwards, the harmonic distortion grows, and the system becomes unstable. Figure 4.8 and Figure 4.9 shows the grid injected currents in ABC domain and Figure 4.10 shows the grid injected current in DQ domain.

At time $t = 3.05s$, the VOI controller is engaged which introduces virtual damping through the shaped impedance. Through, the presence of damping, the harmonic distortions in grid current are damped and the system goes back to its stable state.

The overall control signal before scaling, i.e. PI-control with grid voltage feedforward and VOI controller is shown in Figure 4.11. Without the VOI controller, the traditional PI with feedforward cannot stabilize the system.

The time domain response of the VOI controller is shown in Figure 4.8. For the time less than 3 seconds, it can be seen that the VOI controller is applying higher order harmonics to damp the harmonic interaction between the inverter and grid impedance and when the VOI controller is disengaged at $t = 3s$, the system becomes unstable. At time $t = 3.05$ seconds, the VOI controller is engaged and it can be noted from Figure 4.9 that the VOI controller tries to apply higher order harmonics to damp the resonance.

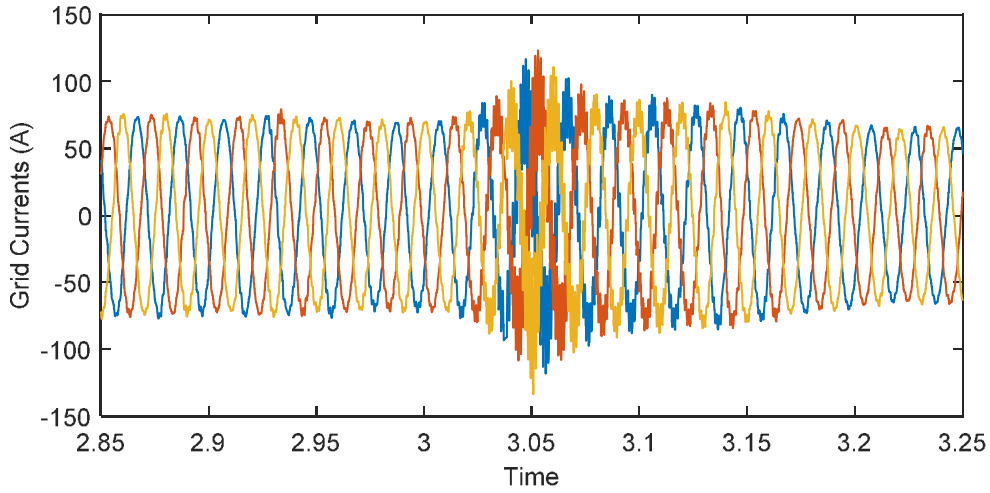

Figure 4.8 Grid Current in ABC frame

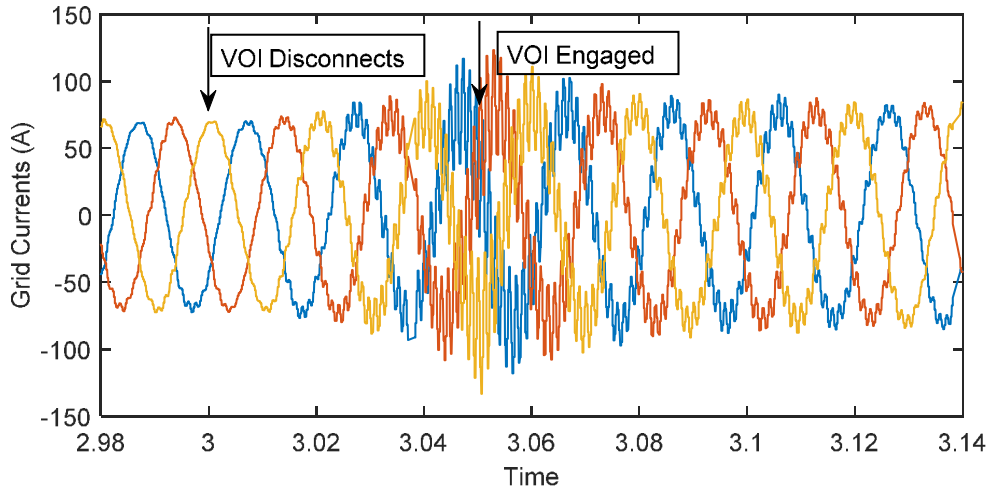

Figure 4.9 Grid Current in ABC Frame (zoomed) - Showing Harmonic Instability due to absence of VOI Controller

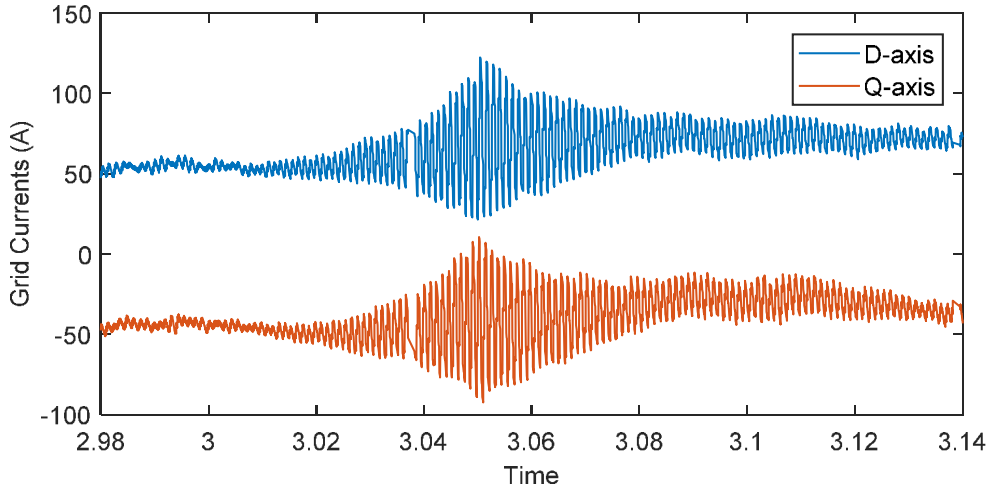

Figure 4.10 Grid Current in DQ Frame (zoomed) - Showing Harmonic Instability due to absence of VOI Controller

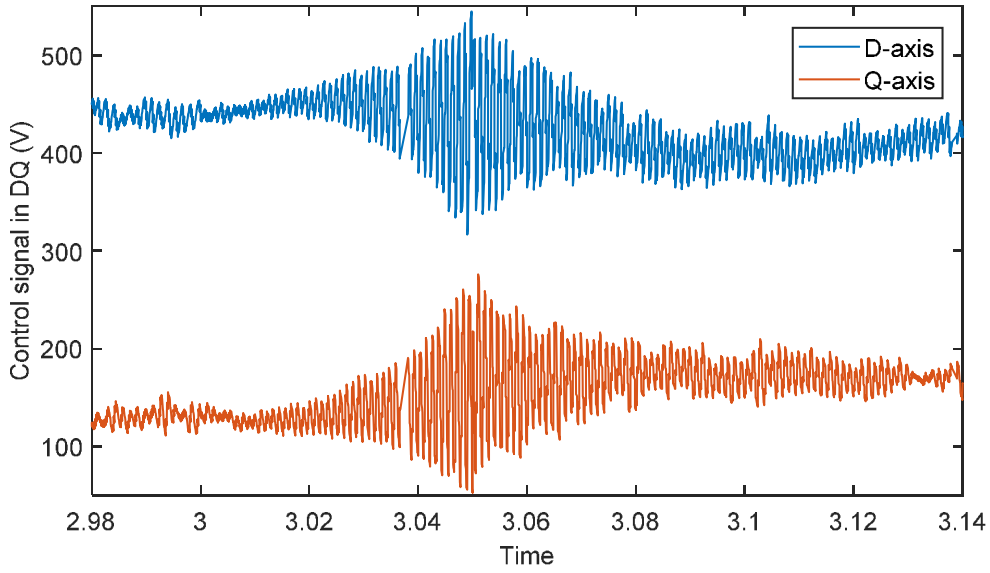

Figure 4.11 Overall controller response (PI+VOI)

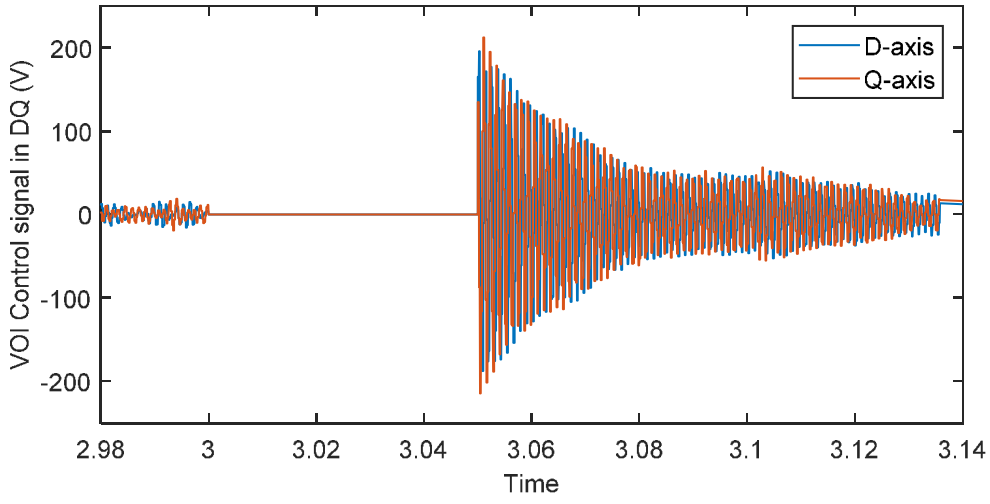

Figure 4.12: VOI Controller Response

5. Conclusion

Four of the control techniques developed in WP2/3 are tested with realistic grid data. Two of these, the voltage control techniques, are implemented in real-time simulations. The advantage of validating in real-time simulations is that field devices and the actual control implementation which should be used in the field can be integrated and tested.

Furthermore, the real-time performance of DPsim, the simulator developed in the frame of the RESERVE project, is evaluated for large grid sizes of several hundred nodes.

What we have achieved is

- real-time simulation based evaluation of the active voltage management (AVM) algorithm of WP3 showing that it improves the voltage band in an LV grid with a high share of renewables
- real-time simulation based evaluation of the dynamic voltage control techniques developed in WP3 demonstrating that it is able to remove harmonic instabilities
- simulation the Romanian and Irish transmission system demonstrating that energy storage systems in combination with WP2 frequency control techniques are beneficial for fast frequency control and transient stability
- successful validation of the frequency maker index to identify power system devices that could participate in inertial response, RoCoF and primary frequency control
- successful validation of the dynamic phasor based real-time simulator DPsim developed in the frame of the RESERVE project for grids of several hundred nodes

6. References

[1] Romanian Wind Energy Association, Online: http://rwea.ro/

[2] Transelectrica, Online: http://www.transelectrica.ro/widget/web/tel/sen-harta/-/harta_WAR_SENOperareHartaportlet

[3] Transelectrica, Network operation. Online: http://transelectrica.ro/web/tel/functionare-retea

[4] Transelectrica, Online: http://www.transelectrica.ro/avize-contracte

[5] C. Murphy, A. Keane, "Local and Remote Estimations Using Fitted Polynomials in Distribution Systems," IEEE Transactions on Power Systems, vol. 32, no. 4, pp. 3185-3194, July 2017.

[6] EirGrid Group, "All island Irish transmission system map." [Online]. Available: http://smartgriddashboard.eirgrid.com/#all/transmission-map

[7] Zárate Miñano, R., and Milano, F. Construction of SDE-based wind speed models with exponentially decaying autocorrelation. Renewable Energy 94 (2016), 186 – 196.

[8] Carta, J., Ramírez, P., and Velázquez, S. A review of wind speed probability distributions used in wind energy analysis: Case studies in the Canary Islands. Renewable and Sustainable Energy Reviews 13, 5 (2009), 933 – 955.

[9] Á. Ortega and F. Milano, "Modeling, simulation, and comparison of control techniques for energy storage systems," IEEETransactions on Power Systems, vol.32, no.3, pp.2445–2454, May 2017.

[10] A.Yazdani and R.Iravani, Voltage-Sourced Converters in Power Systems – Modeling, Control and Applications. Wiley-IEEE Press, 2010.

[11] Á. Ortega and F. Milano, "Stochastic Transient Stability Analysis of Transmission Systems With Inclusion of Energy Storage Devices,"IEEE Trans. On Power Systems, vol.33, no.1, pp. 1077-1079, Jan. 2018.

[12] Mirz, M., Vogel, S., Reinke, G., & Monti, A. (2019). DPsim—A dynamic phasor real-time simulator for power systems. *SoftwareX*, *10*, 100253.

[13] Vogel, S., Mirz, M., Razik, L., & Monti, A. (2017, November). An open solution for next-generation real-time power system simulation. In 2017 IEEE Conference on Energy Internet and Energy System Integration (EI2) (pp. 1-6). IEEE.

[14] F. Milano, 'A Python-based software tool for power system analysis,' in Proceedings of the IEEE PES General Meeting, Vancouver, BC, July 2013.

7. List of Figures

8. List of Tables

9. List of Abbreviations

AIITS	All-Island Irish Transmission System
AVM	Active Voltage Management
AVR	Automatic Voltage Regulation
BESS	Batter Energy Storage System
CSWT	Constant-Speed Wind Turbine
CCT	Critical Clearing Time
DFIG	Doubly-Fed Induction Generators
EMT	Electro Magnetic Transient
ESS	Energy Storage System
FESS	Flywheel Energy Storage System
FRC	Frequency Restoration Control
FCC	Frequency Containment Control
HV	High Voltage
MV	Medium Voltage
LV	Low Voltage
PDF	Probability Density Function
PFC	Primary Frequency Control
PSS	Power System Stabilizer
RoCoF	Rate of Change of Frequency
RoCoP	Rate of Change of Power
SM	Synchronous Machine
SoC	State of Charge
TG	Turbine Governor
ULTC	Under-load Tap Changer
VPP	Virtual Power Plant